XLVI CILAMCE
VITÓRIA - ES - BRAZIL - 2025
XLVI IBERO-LATIN AMERICAN CONGRESS ON COMPUTATIONAL METHODS IN ENGINEERING

Thermo-structural analysis of a timber beam via CS-ASA/FSA

Jackson S. Rocha Segundo[1], Ricardo A. M. Silveira[1], Rafael C. Barros[2], Dalilah Pires[3],
Ígor J. M. Lemes[4], Caroline A. Ferreira[1]

[1]*Dept. of Civil Engineering, Federal University of Ouro Preto*
Morro do Cruzeiro, 35400-000, Ouro Preto/MG, Brazil
jackson.segundo@aluno.ufop.edu.br, ricardo@ufop.edu.br,
caroline.af@aluno.ufop.edu.br, luis.queiroz@aluno.ufop.edu.br
[2]*Concremat Engineering & Tecnology*
Nova Lima, Minas Gerais, Brazil
rafaelcesario@hotmail.com
[3]*Dept. of Technology in Civil Engineering, Computing, Automation, Telematics and Humanities (DTECH), Federal University of São João Del-Rei,*
Campus Alto do Paraopeba Rod.: MG 443, KM 7, 36420-000 Ouro Branco/MG, Brazil
dalilah@ufsj.edu.br
[4]*Dept. of Engineering, Federal University of Lavras,*
Campus Universitário Kennedy, 37200-000 Lavras/MG, Brazil
igor.lemes@ufla.edu.br

Abstract. Timber has gained prominence in contemporary civil construction due to its renewable nature, environmental benefits, and versatility in structural applications. However, its intrinsic combustibility requires careful evaluation of its performance under fire conditions to guarantee safety and reliability in design. This study investigates the thermo-structural response of a glued-laminated timber beam subjected to fire, employing the CS-ASA/FSA (*Computer System for Advanced Structural Analysis/Fire Structural Analysis*), an in-house numerical tool enhanced to incorporate timber-specific formulations. The methodology couples refined plastic hinge and strain compatibility approaches, enabling realistic modeling of stiffness degradation and strength loss under elevated temperatures. Numerical results are compared with experimental and computational data from the literature, demonstrating the accuracy and robustness of the proposed implementation. The findings highlight the critical influence of temperature on the stiffness, strength, and load-bearing capacity of timber beams, reinforcing the importance of advanced numerical tools in predicting fire-induced structural behavior. Overall, the study validates CS-ASA/FSA as an effective framework for evaluating timber elements under fire scenarios, contributing to safer and more sustainable structural design practices.

Keywords: timber, thermo-structural analysis, fire, CS-ASA/FSA, numerical modeling.

1 Introduction

Timber has been widely used as a structural element due to several factors: availability, its renewable and environmentally friendly nature, and the tools that ensure the proper design and sizing of wood-based elements. Because timber is a combustible material, understanding its structural response under fire exposure is essential. When subjected to elevated temperatures, as typically observed in fire scenarios, timber elements experience significant reductions in stiffness and load-bearing capacity. This deterioration results from the progressive degradation of their physical and mechanical properties, which compromises both rigidity and strength during fire exposure.

Understanding the performance of timber structural elements under such extreme conditions is a critical step toward ensuring safe and reliable design. Consequently, the development and application of tools capable of

accurately assessing this behavior are of paramount importance. Traditionally, two main approaches have been adopted for this purpose: experimental testing, which provides direct but often costly and time-consuming insights, and numerical analysis, which offers a flexible and efficient alternative for predicting structural response under fire.

This paper introduces a numerical framework for assessing the behavior of timber structural elements under fire, implemented within the CS-ASA/FSA (*Computer System for Advanced Analysis/Fire Structural Analysis*) [1]. Specific adaptations and extensions were incorporated into the tool to enable accurate modeling of timber structures. The adopted methodology follows the conventional two-stage approach for structural fire analysis. First, a thermal analysis is performed to determine the temperature distribution across the cross-section over time, using a numerical heat transfer procedure that captures the degradation of thermal and mechanical properties with increasing temperature. Subsequently, a thermo-structural analysis evaluates the structural response by incorporating the temperature-dependent material properties obtained in the first stage. To demonstrate and validate the proposed approach, numerical results are presented for a timber beam previously investigated in the literature, enabling direct comparison with experimental and computational benchmarks.

2 Thermo-structural analysis

The structural analysis of wood elements exposed to fire was performed using a beam-column element based on a co-rotational formulation, suitable for tracking significant displacements and rotations. This formulation preserves the local description of the element and allows for efficient representation of geometric nonlinearity. The degradation of stiffness and strength due to fire exposure was addressed through the coupling of the Refined Plastic Hinge Method (RPHM) with the Strain Compatibility Method (SCM). The RPHM captures the initiation and progression of plastic hinges at the ends of structural elements, while the SCM establishes the moment-curvature relationship based on the temperature-dependent mechanical properties of timber. By integrating these approaches, the formulation accounts simultaneously for the nonlinear plastic response and the progressive deterioration of material properties under elevated temperatures, enabling a more realistic representation of structural behavior in fire conditions.

The beam-element stiffness matrix, in incremental form, is given by [2]:

$$\begin{Bmatrix} \Delta P \\ \Delta M_i \\ \Delta M_j \end{Bmatrix} = \begin{bmatrix} \dfrac{EA_{t,i} + EA_{t,j}}{2L} & 0 & 0 \\ 0 & \dfrac{3EI_{t,i} + EI_{t,j}}{L} + \dfrac{2PL}{15} & \dfrac{EI_{t,i} + EI_{t,j}}{L} - \dfrac{PL}{30} \\ 0 & \dfrac{EI_{t,i} + EI_{t,j}}{L} - \dfrac{PL}{30} & \dfrac{EI_{t,i} + 3EI_{t,j}}{L} + \dfrac{2PL}{15} \end{bmatrix} \begin{Bmatrix} \Delta\delta \\ \Delta\theta_i \\ \Delta\theta_j \end{Bmatrix} \tag{1}$$

in which Δ describes incremental variables; *EA* and *EI* are, respectively, the axial and flexural stiffnesses, which will be discussed later; *L* is the element length; *P* is the axial force; δ is the axial displacement; *M* is the resultant bending moment; and θ are the rotations at node *i* and *j*. The terms presented in Eq. (1) already incorporate the effects of geometric nonlinearity [3-5]. Physical nonlinearity is treated at the ends of the finite elements by assuming a linear bending moment gradient along their length. When the internal forces reach the complete yield envelope of the cross-section, the plastic hinge forms, resulting in the cancellation of certain terms of the stiffness matrix. To avoid numerical problems associated with this loss of stiffness, a return mapping strategy is adopted [6], which allows stable re-establishment of equilibrium.

2.1 Cross-sectional analysis

The deformation of the cross-section under internal forces is evaluated in this study using the Strain Compatibility Method (SCM). In this formulation, the axial (*EA*) and flexural (*EI*) stiffnesses in Eq. (1) are obtained from the tangent of the moment-curvature relationship, which depends on the modulus of elasticity derived from the uniaxial constitutive law of the material. Further details on this approach are available in Lemes [7].

To represent the thermal effects on timber, the adopted stress–strain model follows the recommendations of

EN 1995-1-2:2004 [8], which prescribes an elasto-fragile response in tension. However, to enable advanced analyses in both elastic and inelastic ranges, this study employs an elastic-perfectly plastic model for the tensile region. This adaptation captures the progressive deterioration of stiffness and strength with increasing temperature, ensuring a realistic representation of material behavior under fire conditions.

Discretization of the cross-section is required to describe its deformed configuration. In constructing the moment-curvature relationship through the Newton–Raphson method, the area and position of each fiber must be defined. The fiber coordinates (x, y) are referenced to the plastic centroid (PC) of the section, which improves numerical convergence [9]. This discretization allows calculation of the axial strain ε at the PC of each fiber, and, through the constitutive relations, determination of the corresponding stresses, σ_i. Thus, the axial strain in the i^{th} fiber, ε_i, is given by:

$$\varepsilon_i = \varepsilon_0 + \phi\, y_i \tag{2}$$

where y_i is the distance between the plastic centroids of the analyzed fiber and the cross-section; ε_0 and ϕ are respectively the axial deformation in the PC of the section and corresponding curvature.

In the matrix formulation commonly used in numerical procedures, ε_0 and ϕ are treated as components of the deformation vector, where ε_0 and ϕ are treated as components of the deformation vector $\mathbf{X} = [\varepsilon_0 \;\; \phi]^{\text{T}}$. According to Chiorean [10], initializing this vector as null in the first iteration accelerates convergence. Lemes *et al.* [9] further note that, because the cross-section starts from an undeformed state, issues related to the balance between external and internal forces are minimized. Under these conditions, cross-section equilibrium is satisfied when the following equation holds:

$$\mathbf{F}(\mathbf{X}) = \mathbf{f}_{ext} - \mathbf{f}_{int} = \begin{bmatrix} N_{ext} \\ M_{ext} \end{bmatrix} - \begin{bmatrix} N_{int} \\ M_{int} \end{bmatrix} \cong 0 \tag{3}$$

in which the external force vector $\mathbf{f}_{ext}$ is given by the axial force, N_{ext}, and the bending moment, M_{ext}, and the terms N_{int} and M_{int} are the components of the internal force vector, $\mathbf{f}_{int}$.

The internal forces are computed from the deformed configuration of the cross-section using standard integral formulations, expressed as:

$$N_{int} = \iint_{A_w} \sigma_w dA = \sum_{i=1}^{n_{fib,w}} \sigma_{wi} A_{wi} \;\text{ and }\; M_{int} = \iint_{A_w} \sigma_w y dA = \sum_{i=1}^{n_{fib,w}} \sigma_{wi} A_{wi} y_{wi} \tag{4,5}$$

where $n_{fib,w}$ is the number of fibers in the timber cross-section; A_i is the area of the fiber and y_i is the position of the fiber in relation to the PC.

Thus, for the next iteration, k+1, the strain vector is calculated from:

$$\mathbf{X}^{k+1} = \mathbf{X}^k + \mathbf{F}'\left(\mathbf{X}^k\right)^{-1} \mathbf{F}\left(\mathbf{X}^k\right) \tag{6}$$

in which $\mathbf{F}'$ is the Jacobian matrix of the nonlinear problem, that is:

$$\mathbf{F}' = \left(\frac{\partial \mathbf{F}}{\partial \mathbf{X}}\right) = \begin{bmatrix} \dfrac{\partial N_{int}}{\partial \varepsilon_0} & \dfrac{\partial N_{int}}{\partial \phi} \\ \dfrac{\partial M_{int}}{\partial \varepsilon_0} & \dfrac{\partial M_{int}}{\partial \phi} \end{bmatrix} \tag{7}$$

The terms of this Jacobian matrix, $\mathbf{F}'$, of the cross-section are given by the expressions:

$$\begin{aligned} f_{11} &= \frac{\partial N_{int}}{\partial \varepsilon_0} = \int_A E_t dA \cong \sum_{i=1}^{n_{fib}} E_{t,i} A_i; \quad f_{12} = \frac{\partial N_{int}}{\partial \phi} = \int_A E_t y dA \cong \sum_{i=1}^{n_{fib}} E_{t,i} A_i y_i \\ f_{21} &= \frac{\partial M_{int}}{\partial \varepsilon_0} = \int_A E_t y dA \cong \sum_{i=1}^{n_{fib}} E_{t,i} A_i y_i; \quad f_{22} = \frac{\partial M_{int}}{\partial \phi} = \int_A E_t y^2 dA \cong \sum_{i=1}^{n_{fib}} E_{t,i} A_i y_i^2 \end{aligned} \tag{8}$$

where $E_{t,i}$ is the tangent modulus of elasticity taken directly from the constitutive relationship of the component material of the i^{th} fiber. It should be noted that, under fire conditions, the tangent modulus of elasticity is adjusted by a material-specific reduction factor, which, in this study, is applied to timber.

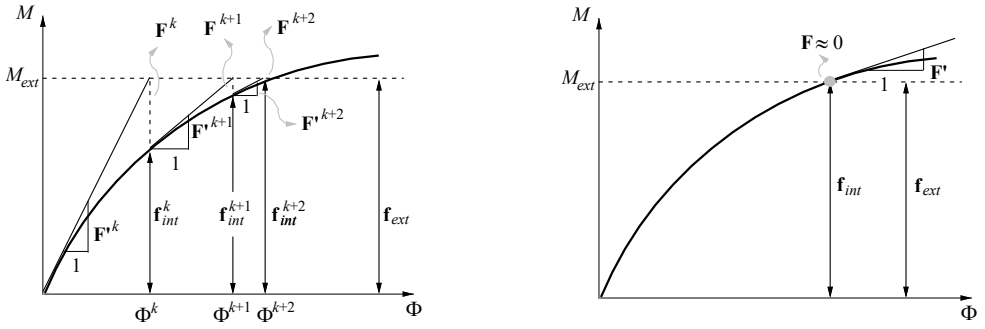
The convergence criterion is defined as the ratio between the Euclidean norms of the unbalanced force vector, **F**, and the external force vector, $\mathbf{f}_{ext}$:

$$\frac{\|\mathbf{F}\|}{\mathbf{f}_{ext}} \leq Tol \tag{9}$$

where *Tol* is the tolerance, set to10^{-5}.

When the convergence criterion is satisfied (Fig. 1a), the system reaches equilibrium. At this stage, the generalized stiffness parameters, EA_t and EI_t, are evaluated from the fiber strains in the deformed configuration. These strains are then used to assemble the Jacobian matrix at equilibrium (Fig. 1b). The expressions for EA_t and EI_t are provide in [9]:

$$EA_t = (f_{11}f_{22} - f_{12}^2)/f_{22} \quad \text{and} \quad EI_t = (f_{11}f_{22} - f_{12}^2)/f_{11} \tag{10,11}$$



a) Iterative process b) Equilibrium point

Figure 1. Moment-curvature relationship [9]

For a given axial force, total plastification of the section occurs when the maximum moment of the moment-curvature relationship is reached. This force pair defines a point on the normal force-bending moment (N-M) interaction curve. The iterative procedure is then repeated for successive bending moment increments until the Jacobian matrix becomes singular. The increment strategy adopted follows the approach proposed by Zubydan [11], namely:

$$M_{n+1} = M_n + d\phi EI_t \tag{12}$$

in which $d\phi$ is a curvature increment, EI_t is the tangent bending stiffness given by Eq. (11), and the sub-indices n and n+1 indicate the current increment and the next increment. The algorithm for obtaining interaction curves is shown in Table 1.

Table 1. Numerical solution adopted to construct the interaction curve

1. Read the section and material data	**15.** Calculate **F(X)**
2. Discretization of the section into fibers	**16.** **if** $\|\mathbf{F}\| \div \|\mathbf{f}_{ext}\| \leq Tol$ **then**
3. Obtaining the plastic centroid (PC)	**17.** Stop the iterative process and go to line 26
4. Translation from the reference system to the PC	**18.** **end if**
5. Determines the maximum axial forces (tension - $N_{t,max}$ e compression - $N_{c,max}$)	**19.** Assembles the tangent stiffness matrix of the section **F'**
6. Calculates the normal effort increment $\Delta N = (N_{t,max} - N_{c,max})/100$	**20.** Checks the uniqueness of **F'**
7. First normal effort value $N = N_{c,max}$	**21.** **if F'** is singular **then**
8. **for** each increment of axial force, *N*, **do**	**22.** The critical bending moment found
9. Initialize **X** = **0**	**23.** Stores *M* and *N* as a point on the interaction curve
10. **for** each increment of bending moment, *M*, **do**	**24.** Stop the process and go to line 29
11. Set $\mathbf{f}_{ext}$	**25.** **end if**
12. **for** $k = 1$, *nmax* **do**	**26.** Corrects the strain vector **X**
13. Determines ε	**27.** **end for**
14. Set $\mathbf{f}_{int}$	**28.** **end for**
	29. $N = N + \Delta N$
	30. **end for**

2.2 Coupling with thermo-structural analysis

In fire scenarios, the structural response is evaluated incrementally in time, allowing simulation of the progressive loss of stiffness and strength as temperature increases. External loads are kept constant during the analysis [12], while thermal effects are incorporated through the temperature-dependent axial and flexural stiffnesses, EA_t and EI_t. Thermal gradients also generate additional strains and stresses, represented by an equivalent nodal force vector, $\mathbf{F}_{ep}$. This vector accounts for both axial elongation and rotations induced by non-uniform temperature distributions across the section, i.e.:

$$\mathbf{F}_{ep}^{\mathrm{T}} = \left[P_T = \sum_{i=1}^{n_{fib,w}} \varepsilon_{th,i} EA_{t,i} \quad 0 \quad M_T = \sum_{i=1}^{n_{fib,w}} \varepsilon_{th,i} y_i EA_{t,i} \right] \tag{13}$$

where ε_{th} is calculated from the thermal expansion recommended by EN 1991-1-5:2003 [13].

The progressive degradation of material properties directly modifies the stiffness matrix and the internal force vector at each time step. In addition, the equivalent thermal forces must be considered in the equilibrium equations, which are solved iteratively using the Newton–Raphson method [4]. Under fire conditions, equilibrium can be expressed as:

$$\mathbf{g} = \mathbf{F}_e + \mathbf{F}_{ep} - \mathbf{F}_i = \lambda \mathbf{F}_r + \mathbf{F}_{ep} - \mathbf{F}_i \cong 0 \tag{14}$$

where $\mathbf{F}_i$ and $\mathbf{F}_e$ are, respectively, the internal and external force vectors. The external vector is obtained from the product of the load parameter λ and the reference load vector, which remains constant throughout the analysis.

The solution proceeds incrementally, ensuring equilibrium at each time step. Figure 2 summarizes the computational procedure for structures under fire. In this flowchart, λ and **U** are the load parameter and the nodal displacements, respectively. The variables obtained at the last equilibrium point are denoted by t, while those calculated at the current point are denoted by $t+\Delta t$; k indicates the current iteration. The superscript 0 identifies the first linear solution within an incremental cycle, while ξ defines the adopted tolerance.

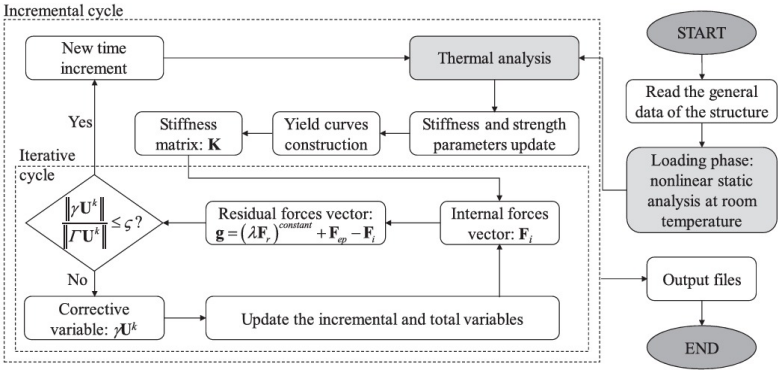


Figure 2. Flowchart of the solution algorithm for thermo-structural analysis in fire situations

3 Numerical validation

This section presents a numerical example that investigates the thermo-structural response of timber elements under fire. The case study considers a two-segment glued-laminated timber beam exposed to elevated temperatures. Originally proposed by Dârmon and Lalu [14], this benchmark problem has been widely used due to the availability of both experimental data and numerical analyses, making it suitable for validating advanced computational models.

Figure 3 shows the physical configuration of the problem, including the main geometric parameters and boundary conditions adopted in the numerical model. For consistency and validation, the same beam geometry, loading, and fire exposure conditions described in the reference study are reproduced. The beam spans 3500 mm and is subjected to a uniformly distributed load of 6,10 kN/m. Fire exposure is simulated on three faces, while the upper surface is protected with thermal insulation. The char layer is defined by the 300 °C isotherm, in accordance

with common practice reported in the literature.

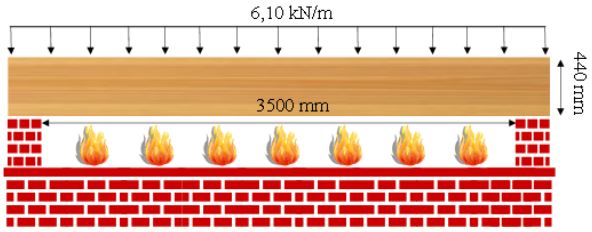


Figure 3. Geometry, loading, and fire exposure conditions of the timber beam model

The thermo-structural analysis was carried out by discretizing the beam into 10 beam–column finite elements and adopting an elasto–perfectly plastic constitutive model. The tensile and compressive moduli of elasticity were assumed equal, $E_t = E_c = 9{,}6$ GPa. The yield stresses were defined $f_{y,t} = 19{,}2$ MPa in tension and $f_{y,c} = 24$ MPa in compression, with corresponding yield strains $\varepsilon_{y,t} = \varepsilon_{y,c} = 2\%$.

For the simply supported beam under uniform loading, the midspan vertical displacement was selected as the primary performance indicator, as this section experiences the maximum bending moment. Figure 4 presents the displacement-time curve under fire exposure, comparing the results of the present study with the experimental and numerical data reported by Dârmon and Lalu [14]. The CS-ASA/FSA predictions show good agreement, lying between the reference experimental and numerical responses. This consistency demonstrates both the robustness of the implemented formulations and the reliability of the proposed numerical framework. The differences observed between the models stem from the distinct thermal formulations employed. SAFIR adopts an enthalpy-based approach, whereas CS-ASA/FSA models the temperature field using specific heat. This methodological divergence leads to variations in the predicted thermal behavior and, consequently, in the structural response.

Figure 5 illustrates the evolution of the beam's load-bearing capacity over fire exposure time, consolidating the thermo-structural analysis and emphasizing the influence of thermal effects on the global structural response. For comparison, the results reported by Dârmon and Lalu [14] for both advanced and simplified models are also included. The response obtained with CS-ASA/FSA shows close agreement with the advanced model, confirming the consistency and accuracy of the proposed formulation.

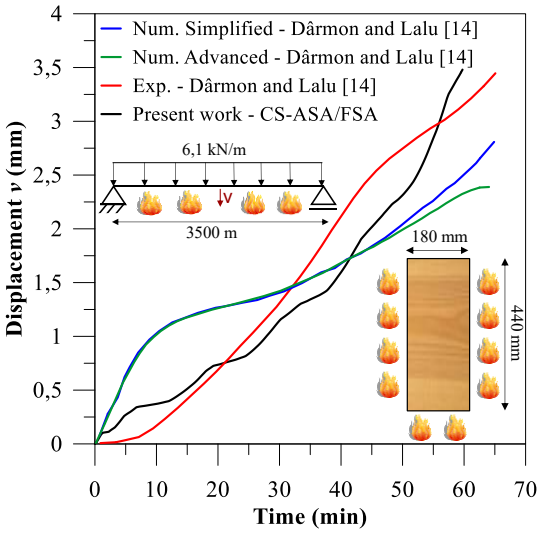


Figure 4. Evolution of midspan displacement under fire exposure compared with reference data

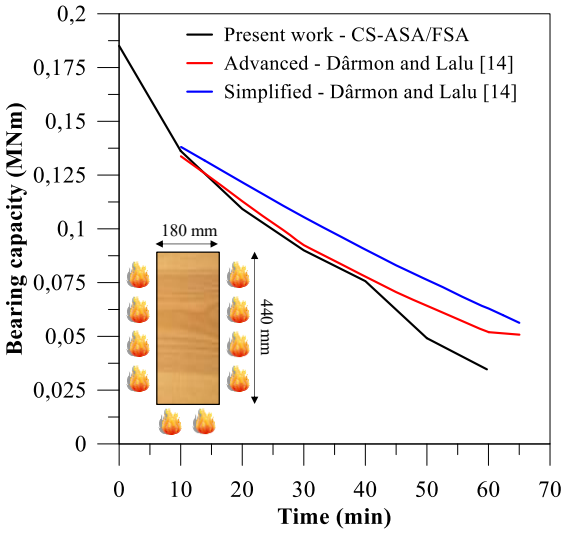


Figure 5. Evolution of beam resistance under fire exposure and comparison with literature models

Overall, the numerical results demonstrate the effectiveness of the CS-ASA/FA and CS-ASA/FSA implementations in capturing the behavior of glued-laminated timber beams under fire. The displacement-time curves clearly reveal the progressive loss of capacity due to section char formation and the temperature-dependent degradation of the wood's mechanical properties. These findings validate the robustness of the proposed methodology and its applicability to the structural analysis of timber elements in fire scenarios.

4 Conclusions

This study implemented and applied a numerical framework within CS-ASA/FSA to evaluate the thermo-structural behavior of glued-laminated timber beams under fire exposure. By coupling the RPHM with the SCM, the model simultaneously captured the formation and progression of plastic hinges and the degradation of material properties as a function of temperature. This integration allowed for a realistic and consistent simulation of stiffness reduction, strength loss, and overall structural response during fire scenarios.

The results demonstrated good agreement with experimental and computational data reported in the literature. The displacement-time and resistance-time curves obtained in this work validated the accuracy of the proposed methodology, with the CS-ASA/FSA framework reproducing the progressive degradation of the cross-section due to charring and the temperature-dependent reduction of mechanical properties. These outcomes confirm the robustness of the adopted formulations and highlight the potential of the proposed approach as a reliable complement to experimental testing, which is often costly, time-consuming, and limited in scope.

Although effective, the present study focused on a specific beam configuration, boundary conditions, and a standardized fire scenario. Future developments should extend the methodology to more complex structural systems, including frames, connections, and multi-span members, as well as to natural fire curves and localized heating conditions. In addition, the integration of CS-ASA/FSA into performance-based design workflows represents a promising step toward advancing fire safety engineering and promoting the safe and sustainable use of timber in modern construction.

Acknowledgements. This research was supported by CAPES, CNPq, FAPEMIG, PROPEC/UFOP, PROPPI/UFOP, UFSJ, UFLA, and the Gorceix Foundation.

Authorship statement. The authors hereby confirm that they are the sole liable persons responsible for the authorship of this work, and that all material that has been herein included as part of the present paper is either the property (and authorship) of the authors, or has the permission of the owners to be included here.

References

[1] R. C. Barros, D. Pires, Í. J. M. Lemes, P. A. S. Rocha and R. A. M. Silveira, "Análise termomecânica de estruturas de aço via acoplamento MCD/MRPR". *XXXVII Ibero-Latin American Congress on Computational Methods in Engineering*, Brasília, DF, Brasil, 2016.

[2] Lemes, Í.J.M.; Silveira, R.A.M.; Silva, A.R.D.; Rocha, P.A.S. – "Nonlinear analysis of two-dimensional steel, reinforced concrete and composite steel concrete structures via coupling SCM/RPHM", *Engineering Structures*, vol. 147, pp. 12-26.

[3] Pires, D.; Barros, R.C.; Silveira, R.A.M.; Lemes, Í.J.M.; Rocha, P.A.S. – "An efficient inelastic approach using SCM/RPHM coupling to study reinforced concrete beams, columns and frames under fire conditions", *Engineering Structures*, vol. 219, pp. 1-25, 2020.

[4] Barros, R.C.; Pires, D.; Silveira, R.A.M.; Lemes, Í.J.M.; Rocha, P.A.S. – "Advanced inelastic analysis of steel structures at elevated temperatures by SCM/RPHM coupling", *Journal of Constructional Steel Research*, vol. 145, pp. 368-385, 2018.

[5] Yang, Y.B.; Kuo, S.B.; *Theory and Analysis of Nonlinear Framed Structures*. Singapore: Prentice Hall; 1994.

[6] Lemes, Í.J.M.; Silveira, R.A.M.; Teles, L.O.M.; Barros, R.C.; Silva, A.R.D. – "Numerical formulation for advanced non-linear static analysis of semi-rigid planar steel frames", *Journal of the Brazilian Society of Mechanical Sciences and Engineering*, vol. 45, 2023.

[7] Lemes, Í.J.M. – Estudo numérico avançado de estruturas de aço, concreto e mistas. Tese de Doutorado, Programa de Pós-Graduação em Engenharia Civil, DECIV/EM/UFOP, Ouro Preto, MG, Brasil, 2018.

[8] EN 1995-1-2:2004. *Eurocode 5: Design of timber structures. Part 1-2: General – Structural fire design*, European Committee for Standardization. Brussels, 2004.

[9] Lemes, Í.J.M.; Silva, J.L.; Batelo, E.A.P.; Silveira, R.A.M.; – "Influence of residual stress models prescribed in design codes for steel I-section behavior", *Revista Internacional de Metodos Numericos para Calculo y Diseno en Ingenieria*, vol. 38, n° 4, 2022.

[10] C. G. Chiorean, "A computer method for nonlinear inelastic analysis of 3D composite steel-concrete frame structures". *Engineering Structures*, vol. 57, pp. 125-152, 2013.

[11] A. H. Zubydan, "Inelastic large deflection analysis of space steel frames including H-shaped cross sectional members". *Engineering Structures*, vol. 48, pp. 155-165, 2013.

[12] Najjar, S.R. – Three-dimensional analysis of steel frames and sub-frames in fire. Ph.D. Dissertation, University of Sheffield, Sheffield, 1994.

[13] EN 1991-1-5:2003. Eurocode 1: Actions on structures. Part 1-5: General actions – Thermalactions, European Committee for Standardization. Brussels, 2003.

[14] Dârmon, R., Lalu, O., 2019. The fire performance of Cross Laminated Timber beams. *Procedia Manufacturing*, 32, 121-128.